ISSN: 2633-4828 Vol. 8 No.1, January, 2026

International Journal of Applied Engineering & Technology

COMPARATIVE ANALYSIS OF MAGNETOTELLURIC IMPEDANCE TENSOR ESTIMATION METHODS USING SYNTHETIC AND FIELD DATA

B. Pradeep Naick*[1], K. Naganjaneyulu[2] and I. Santi Prabha[3]

*[1]Instrumentation, Airborne & Engineering Geophysics, CSIR-National Geophysical Research Institute, Hyderabad 500 007, Telangana, India

[2]Electromagnetic Geophysics, CSIR-National Geophysical Research Institute, Hyderabad 500 007, Telangana, India

[3]Department of Electronics and Communication Engineering, JNTU Kakinada, Kakinada 500 007, Andhra Pradesh, India

*kholapradeep@gmail.com

ABSTRACT

The impedance tensor relates electric and magnetic fields and must be estimated from noisy time series data accurately. This paper presents a systematic comparison of three methods used to calculate MT impedance tensors. The first method uses standard spectral averaging, which is fast but sensitive to noise. The second method applies least squares regression, which is more stable for overdetermined systems. And, the third method uses robust M-estimation with Huber weighting to down-weight outliers automatically. We tested all three methods using synthetic data with a known 1D impedance response. And, these synthetic validations were then complemented by applying all three strategies to field MT data from the Dharwar craton, Karnataka, India. We applied coherency-based segment selection to remove uncorrelated data prior to processing, and bootstrap resampling was used to provide error estimates for each method. The results indicate that the robust method performed better than the other two conventional approaches. While all three methods successfully recovered impedance when applied to clean synthetic data, field data analysis showed performance differences. This integrated field-synthetic approach provides MT practitioners with practical tools for method selection, quality control, and realistic uncertainty estimation.

Keywords: *Magnetotellurics, Dharwar Craton, Impedance Tensor Estimation, Standard Averaging, Least Squares, Robust Regression, Coherency, Bootstrap Resampling*

1. INTRODUCTION

The magnetotelluric (MT) method is a passive electromagnetic geophysical technique which measures natural variations in Earth's electric and magnetic field to interpret subsurface electrical resistivity structure (Vozoff, 1991; Simpson and Bahr, 2005). From the introduction by Tikhonov (1950) and Cagniard (1950), MT has turned into a vital tool for investigating the Earth's crust and mantle. The method's capacity to penetrate deeper depths without the need for active sources makes it valuable for exploring complex geological environments where other geophysical methods face limitations (Berdichevsky and Dmitriev, 2008).

The fundamental challenge in MT data processing is estimating the impedance tensor correctly, which is associated with measured horizontal electric fields to horizontal magnetic fields in the frequency domain (Caldwell et al., 2004). This impedance tensor contains all information about subsurface resistivity structure and needs to be extracted from time-series measurements contaminated by various noise sources (Jones, 2012). Three essential approaches have emerged for impedance estimation: Standard averaging of cross-power spectral densities, Least squares solution of overdetermined systems, and Robust regression using iterative reweighting (Sims et al., 1971; Stodt, 1983; Egbert, 1997). Though all three methods attempt to fix the same fundamental problem, they differ significantly in how they handle noise, outliers, and data quality variations, which are unavoidable in real-world measurements.

The choice of impedance estimation method is not merely a technical detail but fundamentally affects data quality, interpretation reliability, and ultimately the accuracy of subsurface models derived from MT surveys

(Chave and Thomson, 2004). Early MT processing relied on simple spectral averaging techniques that assumed Gaussian noise distributions and stationary statistics (Goubau et al., 1978). Though, field measurements break these assumptions due to cultural electromagnetic interference from power lines, railways, and industrial facilities, in urban and semi-urban environments especially (Kappler, 2012; Szarka and Menvielle, 1997). These contaminating sources produce non-Gaussian noise and outliers that can bias conventional processing methods seriously (Larsen, 1989).

These limitations resulted in the development of robust statistical approaches for MT impedance estimation. Egbert and Booker (1986) introduced bounded-influence estimation techniques that down weight outlier-contaminated data segments, by improving the results in noise environments. Despite these theoretical advances, systematic quantitative comparisons of different impedance estimation methods using both synthetic validation and real field data remain surprisingly rare in the published literature (Jones and Jodicke, 1984). Most studies focus on introducing new techniques rather than comparing existing approaches under controlled conditions (Gamble et al., 1979).

Several important questions remain incompletely addressed: For impedance tensor estimation, how much do processing method choices matter? In what conditions does each method achieve better results? Can synthetic data testing predict field data results? These questions have practical effects for MT practitioners who need to choose processing approaches without clear guidance on expected results (Wight et al., 1977).

This study addresses the gaps through a comparative analysis of the three impedance estimation methods - standard averaging, Least squares optimization, and Robust iterative processing. We applied a dual verification strategy, combining synthetic data with known impedance responses and field data from the Dharwar craton, Karnataka, India. The synthetic testing confirms the algorithmic performance of three methods, whereas field data analysis shows how the methods deal with real-world contamination. We evaluated the performance of these methods using bootstrap resampling which provides realistic uncertainty estimates.

This paper is organized as follows: Section 2 presents the theoretical background on impedance tensors, apparent resistivity, phase and uncertainty estimation. Section 3 describes the methodology for all three impedance estimation methods, including data pre-processing, algorithm implementation, bootstrap error estimation. Section 4 validates the methods using synthetic data generated from a three-layer earth model, confirming algorithmic correctness under ideal conditions. Section 5 presents field data analysis from the Dharwar craton, Karnataka, India, which quantifies method performance differences and identifies frequency-dependent error patterns. Section 6 presents conclusions and recommendations for MT practitioners operating in electromagnetically noisy environments.

2. THEORY

2.1 MT Fundamentals

Maxwell's equations describe the interaction between time-varying electric and magnetic fields in a conductive Earth that can be defined in the frequency domain. Under the plane wave assumption, these equations yield a linear relationship between the horizontal electric and magnetic field components at the Earth's surface, which is generally valid for most regional magnetotelluric investigations. This relationship, comprising four elements, is expressed through a frequency-dependent complex impedance tensor that describes the subsurface electromagnetic response.

$$\nabla \times E = -i\omega\mu_0 H, \nabla \times H = \sigma E, \quad (1)$$

And, using the plane-wave assumption, the MT impedance tensor is defined as:

$$Z(\omega) = \begin{bmatrix} Z_{xx} & Z_{xy} \\ Z_{yx} & Z_{yy} \end{bmatrix} \quad (2)$$

2.2 Magnetotelluric Data Acquisition

Magnetotelluric (MT) method uses natural electromagnetic waves from the Earth's atmosphere and space. Lightning storms and solar wind create electromagnetic signals continuously. These waves penetrate into the earth's subsurface at different depths depending on their frequency. Low-frequency waves penetrate deeper, whereas high-frequency waves stay near the surface. MT stations record both electric and magnetic field variations at the earth's surface at the same time. Electric fields are acquired and recorded using induction coils or fluxgate magnetometers. MT data is recorded for several hours to several days, and the recording interval relies on the desired depth of investigation. Longer recording times catch lower frequencies and explore deeper structures. Modern MT systems digitize data at sampling rates from less than 1 Hz to several thousand Hz. Five components are recorded: two horizontal electric fields (Ex, Ey) and three magnetic fields (Hx, Hy, Hz). The recorded time series data further processed to estimate the impedance tensors. These impedance values uncover the electrical resistivity structure below the measurement site.

2.3 Spectral Estimation for Standard Averaging Method

Impedance estimation depends on reliable spectral estimates of the time-series data, which is performed in the frequency domain. The most common approach uses the Fast Fourier Transform (FFT) to convert each time segment from time domain to frequency domain. However, simple FFT-based spectra have problems: spectral leakage (i.e. energy spreading to neighbouring frequencies) and high variance (noisy, unstable estimates), particularly when data segments are short or contaminated by noise (Percival and Walden, 1993). To improve spectral quality, we applied windowing to each time segment before computing the FFT. Windowing reduces spectral leakage by tapering the data to zero at segment boundaries, preventing abrupt discontinuities. The Hanning window (also called Hann window) is used, which provides a good balance between reducing leakage and maintaining frequency resolution. The averaging process significantly reduces variance, and in the standard averaging method, the result is a more stable and reliable spectral estimate, which is the basis for impedance calculation. The windowed time-series is transformed to the frequency domain using FFT, and the power spectral density quantifies the signal strength at each frequency and is computed as:

$$X(\omega) = \sum_{t} x(t)v(t)e^{-i\omega t}, \quad S_{xx}(\omega) = \frac{1}{N}|X(\omega)|^2 \tag{3}$$

Where, x(t) is the time segment, v(t) is hanning window, X(ω) is the FFT, $S_{xx}(\omega)$ is the power spectral density, N is the segment length.

2.4 Auto and cross power spectral matrices

Spectral estimates are used to construct auto- and cross-power spectral matrices for electric and magnetic field components. The magnetic auto-power matrix describes the energy and correlation between magnetic components. And, the electric-magnetic cross-power matrix catches the inductive coupling between the fields (Egbert and Booker, 1986). These matrices provide a compact statistical representation of the MT data at each frequency and serve as the basis for impedance estimation using regression techniques. For each segment and each taper, auto and cross-power spectral matrices are written as:

$$S_{HH} = \begin{bmatrix} S_{H_xH_x} & S_{H_xH_y} \\ S_{H_yH_x} & S_{H_yH_y} \end{bmatrix}, \quad S_{EH} = \begin{bmatrix} S_{E_xH_x} & S_{E_xH_y} \\ S_{E_yH_x} & S_{E_yH_y} \end{bmatrix} \tag{4}$$

2.5 Coherency

Coherency measures the linear correlation between two signals as a function of frequency and is popularly used as a data quality indicator in MT processing. Coherence between channels X and Y is defined as:

$$\gamma^2 = \frac{|S_{XY}|^2}{S_{XX}S_{YY}} \tag{5}$$

Where S_{XX} and S_{YY} are auto-spectra, and S_{XY} is the cross-spectrum (Egbert and Booker, 1986).

Low coherency indicates noise contamination or non-inductive effects. Such data segments are down-weighted or rejected to improve the reliability of impedance estimates.

2.6 Least Squares Impedance Estimation

The least squares (LSQ) regression is used for conventional MT impedance estimation, which minimises the difference between the observed and predicted electric fields.

From the linear model E=ZH, LSQ gives:

$$Z = (H^H H)^{-1}(H^H E) \qquad (6)$$

where superscript H denotes the Hermitian transpose (Gamble et al., 1979).

LSQ estimation is efficient and straightforward, but it is sensitive to outliers and assumes ideal noise conditions, which are neglected in real MT data.

2.7 Robust Regression (M-Estimation)

Robust regression methods are better than LSQ by reducing the influence of outliers and non-Gaussian noise. This is achieved by applying weights to the residuals between observed and predicted electric fields, thereby large residuals receive less influence during estimation (Huber, 1981; Tukey, 1977). The impedance tensor is iteratively estimated using a weighted least-squares formulation: Residuals

$$r = E - ZH \qquad (7)$$

A weight function w(r) (e.g., Huber weight) is applied iteratively until convergence.

$$Z_{robust} = (H^H W H)^{-1}(H^H W E) \qquad (8)$$

Where W is a diagonal weight matrix. Robust regression provides more stable estimates in the presence of spikes and cultural noise.

2.8 Bootstrap resampling

Accurate uncertainty estimation is essential for magnetotelluric data interpretation and inversion. Traditional error estimation methods assume Gaussian noise distributions, which may not reflect real-world conditions where outliers and non-Gaussian noise are common (Chave and Thomson, 2004). We applied bootstrap resampling (Efron and Tibshirani, 1993), a non-parametric statistical method that estimated uncertainties without requiring assumptions about error distributions.

Bootstrap resampling generates multiple synthetic datasets by randomly resampling the original data with replacement (Davison and Hinkley, 1997). Each synthetic dataset, called a bootstrap sample, has the same size as the original but contains some repeated segments and neglects others. The impedance estimation method is applied to each bootstrap sample, creating multiple realizations of the impedance tensor. The variability across these realizations provides a realistic estimate of uncertainty (Jones and Jodicke, 1984).

$$\sigma\_\rho = \sqrt{[1/(N_{boot} - 1)\sum(\rho_i^* - \rho^*)^2]} \qquad (9)$$

where ρ_i^* is the apparent resistivity from bootstrap iteration i, and ρ^* is the mean across all iterations.

2.9 Apparent Resistivity and Phase:

The magnetotelluric impedance tensor Z is a complex quantity that relates the horizontal electric and magnetic fields at Earth's surface (Cagniard, 1953). While impedance provides complete information about the electromagnetic response, it is not directly interpretable in terms of subsurface resistivity structure. Therefore, we convert impedance to two physically meaningful quantities: apparent resistivity and phase (Vozoff, 1991).

Apparent resistivity ρ_a represents the resistivity of a homogeneous half space that would produce the same impedance as the actual layered or heterogeneous Earth (Simpson and Bahr, 2005). It is calculated from the impedance magnitude using Cagniards formula (Cagniard, 1953):

$$\rho_a = \frac{|Z_{xy}|^2}{\mu_0 \omega} \quad (10)$$

where, ρ_a is apparent resistivity (Ω·m), μ_0 = 4π × 10^{-7} H/m is magnetic permeability of free space, ω = 2πf is angular frequency (rad/s) and $|Z_{xy}|$ is impedance magnitude (mV/km/nT)

The impedance phase ϕ represents the time lag between electric and magnetic field variations (Berdichevsky and Dmitriev, 2008). For a purely resistive Earth, electric and magnetic fields would be exactly in phase (ϕ =0°). For a realistic Earth with both resistive and inductive properties, the phase ranges between 0° and 90° (Weaver et al., 2000).

$$\phi = \tan^{-1}\left(\frac{I(Z_{xy})}{R(Z_{xy})}\right) \quad (11)$$

Where, $I(Z_{xy})$ and $R(Z_{xy})$ are the imaginary and real parts of the complex impedance, and the result is converted from radians to degrees.

3. METHODOLOGY

This section describes the three impedance tensor estimation methods implemented for magnetotelluric data processing: Standard, Least Squares, and Robust. All three methods operate in the frequency domain and aim to estimate the impedance tensor Z from measurements of electric field E and magnetic field B, but differ in how they handle noise and outliers.

3.1 Data Pre-processing

Before applying any estimation method, the continuous time-series data undergoes several pre-processing steps:

3.1.1 Segmentation

The recorded time-series data is divided into n segments of equal length. Each segment should contain at least several periods of the longest-period signal of interest to ensure adequate frequency resolution. In this study, we used segments of 4096 samples each, providing frequency coverage from approximately 0.0002 Hz to 0.5 Hz with a sampling rate of 1 Hz.

3.1.2 Fourier Transformation

Each time-series segment is transformed from the time domain to the frequency domain using the Fast Fourier Transform (FFT). This converts the time-varying electric field E(t) and magnetic field B(t) measurements into their frequency-domain representations E(f) and B(f) for each segment.

3.1.3 Power Spectral Density Calculation

For each segment and each frequency, we calculate the auto-power and cross-power spectral densities between electric and magnetic field components, i.e., S_EB(f) is the Cross-power between electric field E & magnetic field B, and S_BB(f) is the Auto-power of magnetic field B. These spectral densities form the basis for impedance estimation in all three methods.

3.1.4 Coherency-Based Quality Control

Prior to impedance estimation, we calculate the coherency between electric and magnetic field components for each segment. Coherency measures how well the electric field correlates with the magnetic field at each frequency and ranges from 0 (no correlation) to 1 (perfect correlation). Segments with coherency below a specified threshold are rejected as they likely contain excessive noise or interference that would contaminate the impedance estimates. This quality control step confirms that, only reliable data segments contribute to the final impedance tensor calculation.

3.2 Standard Method

3.2.1 Principle

The standard method is the most straightforward approach, based on averaging cross-power spectral densities across all accepted time segments before calculating the impedance tensor. This method assumes that noise is random and uncorrelated between segments, so averaging reduces its impact.

3.2.2 Algorithm

For each frequency f:

Step 1: Calculate cross-power and auto-power spectra for each segment:

Segment 1: S_EB(1,f), S_BB(1,f)

Segment 2: S_EB(2,f), S_BB(2,f)

...

Segment n: S_EB(n,f), S_BB(n,f)

Step 2: Average the spectral densities across all n segments:

$S\_EB\_avg(f) = (1/n) \times \Sigma\ S\_EB(i,f)$

$S\_BB\_avg(f) = (1/n) \times \Sigma\ S\_BB(i,f)$

Step 3: Calculate impedance tensor by matrix division:

$Z(f) = S\_EB\_avg(f) \times [S\_BB\_avg(f)]^{(-1)}$

Step 4: Convert impedance to apparent resistivity and phase

Apparent resistivity $\rho(f) = (1/\mu_0\omega)\ |Z(f)|^2$

Phase $\varphi(f) = \arctan[Im(Z(f)) / Re(Z(f))]$

Where μ_0 is the magnetic permeability of free space and $\omega = 2\pi f$ is angular frequency

The standard method works well when the noise is Gaussian and uncorrelated. It assumes all segments have equal quality, and it is sensitive to outliers (a single contaminated segment affects the average). And also, this method cannot handle non-Gaussian noise effectively.

3.3 Least Squares Method

3.3.1 Principle

The Least Squares method treats impedance estimation as an optimization problem. Finding the impedance tensor that minimizes the squared differences between observed and predicted electric fields across all segments simultaneously. Unlike the standard method that averages first, this approach uses all segment information at once to find the optimal solution.

3.3.2 Algorithm

For each frequency f:

Step 1: Stack frequency-domain electric and magnetic field data from all segments:

E_stack = [E(1,f); E(2,f); ...; E(n,f)] (n×2 matrix: Ex, Ey)

B_stack = [B(1,f); B(2,f); ...; B(n,f)] (n×2 matrix: Bx, By)

Step 2: Formulate the overdetermined system:

E_stack = Z(f) × B_stack

This creates a system with n equations (one per segment) and 4 unknowns (the four components of the 2x2 impedance tensor)

Step 3: Solve using pseudoinverse (least squares solution):

Z(f) = [B_stack^H × B_stack]^(-1) × B_stack^H × E_stack

Where ^H denotes the Hermitian transpose (complex conjugate transpose).

Step 4: Convert to apparent resistivity and phase using the same formulas as the standard method.

The LSQ method uses all data simultaneously; it is optimal for Gaussian noise and naturally handles over determined systems. This method remains sensitive to outliers and also assumes that errors are Gaussian distributed. A few bad segments can heavily influence the results.

3.4 Robust Method

3.4.1 Principle

The Robust method addresses the outlier sensitivity of standard and Least squares methods by iteratively identifying and down weighting contaminated data segments. It uses Iteratively Reweighted Least squares (IRLS) with a Huber M-estimator to assign lower weights to segments with large residuals (likely outliers) and higher weights to segments with small residuals (likely good data).

3.4.2 Algorithm

For each frequency f:

Step 1: Initialize with Least squares solution:

$Z_0(f)$ = Least Squares solution

Step 2: Begin iterative reweighting loop:

Iteration k:

a) Calculate residuals for each segment:

residual(i) = |E(i,f) - Z_k(f) × B(i,f)|

b) Calculate Median Absolute Deviation (MAD) as robust scale estimate:

MAD = 1.4826 x median(|residuals - median(residuals)|)

The factor 1.4826 makes MAD consistent with standard deviation for Gaussian noise.

c) Calculate weights using Huber function with tuning parameter c = 2.5:

For each segment i:

If |residual(i)| / MAD ≤ c:

weight(i) = 1

else:

weight(i) = (c x MAD) / |residual(i)|

This assigns weight = 1 to good data (small residuals) and weight < 1 to outliers (large residuals).

d) Solve weighted least squares problem:

Z_(k+1)(f) = [B^H × W × B]^(-1) × B^H × W × E

Where W is a diagonal matrix with weights on the diagonal

e) Check convergence:

If |Z_(k+1) - Z_k| / |Z_k| < 10^(-6):

converged → stop

else:

continue to next iteration

Step 3: Maximum 20 iterations allowed. If not converged, use the last iteration result.

Step 4: Convert to apparent resistivity and phase.

3.4.2 Tuning Parameter Selection

The Huber tuning parameter c = 2.5 is chosen based on standard recommendations:

c = 1.345: High outlier rejection (95% efficiency for Gaussian noise)

c = 2.5: Moderate outlier rejection (used in this study, balances robustness and efficiency)

c = 4.0: Mild outlier rejection (99% efficiency for Gaussian noise)

We selected c = 2.5 to provide strong outlier resistance while maintaining good performance on clean data.

The robust method is highly resistant to outliers and non-Gaussian noise; it automatically identifies and down weights bad data. It converges to the Least squares solution when no outliers are present. The performance of this method depends on the tuning parameter choice and can be extremely aggressive if the threshold is set too low.

3.5 Bootstrap Error Estimation

All three methods require uncertainty estimates to assess the data quality and weight inversions. We used bootstrap resampling to estimate errors without assuming a specific statistical distribution.

3.5.1 Bootstrap procedure

Step 1: From **n** available segments after coherency filtering, randomly select n segments with

replacement (some segments may be selected multiple times, others not at all).

Step 2: Apply the chosen impedance estimation method (Standard, Least Squares, or Robust) to this resampled dataset.

Step 3: Store the resulting impedance tensor, apparent resistivity, and phase

Step 4: Repeat steps 1-3 for 200 iterations, creating 200 bootstrap realizations.

Step 5: Calculate error estimates:

Error = standard deviation of 200 bootstrap realizations

Step 6: Calculate 95% confidence intervals:

Lower bound = 2.5th percentile of bootstrap distribution

Upper bound = 97.5th percentile of bootstrap distribution

3.6 Impedance Tensor Components

The magnetotelluric impedance tensor **Z** is a 2×2 complex matrix relating horizontal electric and magnetic fields:

$$\begin{bmatrix} Ex \\ Ey \end{bmatrix} = \begin{bmatrix} Zxx & Zxy \\ Zyx & Zyy \end{bmatrix} \begin{bmatrix} Bx \\ By \end{bmatrix} \quad (12)$$

For this study, we focus on the off-diagonal components:

Zxy: Relates Ex (north electric field) to By (east magnetic field)

Zyx: Relates Ey (east electric field) to Bx (north magnetic field)

In a 1D layered Earth, the diagonal components (Zxx, Zyy) should theoretically be zero, and all information is contained in the off-diagonal components. For 2D and 3D structures, off-diagonal components still provide the most reliable impedance information, while diagonal components are more susceptible to galvanic distortion.

3.6.1 Apparent Resistivity and Phase

Each impedance component is converted to:

Apparent Resistivity (Ω·m):

$$\rho_{xy} = \left(\frac{1}{\mu_0 \omega}\right) |Z_{xy}|^2$$

$$\rho_{yx} = \left(\frac{1}{\mu_0 \omega}\right) |Z_{yx}|^2$$

Phase (degrees):

$$\varphi_{xy} = \arctan\left(\frac{\mathrm{Im}(Z_{xy})}{\mathrm{Re}(Z_{xy})}\right)$$

$$\varphi_{yx} = \arctan\left(\frac{\mathrm{Im}(Z_{yx})}{\mathrm{Re}(Z_{yx})}\right)$$

These quantities are physically meaningful and directly used in MT interpretation and inversion.

4. SYNTHETIC DATA TEST

Before applying the three impedance estimation methods to real field data, we validated their performance using synthetic data which is generated with known impedance responses (Weidelt, 1972). Synthetic data testing is important for understanding algorithmic behaviour and establishing performance baselines before field data application (Chave and Thomson, 2004; Wait, 1982). A method, as described by Larsen et al. (1996), is used to generate the synthetic time-series data.

4.1 One-Dimensional Earth Model

We constructed a three-layer 1D Earth model (shown in Figure 1) representing a typical crustal resistivity structure (Jin Chen, 2012):

1. Layer 1 (0-1 km depth): Resistivity ρ_1 = 10 Ω·m (sedimentary cover)
2. Layer 2 (1-3 km depth): Resistivity ρ_2 = 1 Ω·m (conductive layer)
3. Layer 3 (>3 km depth): Resistivity ρ_3 = 1000 Ω·m (resistive basement)

This one-dimensional layered configuration produces apparent resistivity and phase responses, which are appropriate for testing impedance estimation algorithms (Cagniard, 1953).

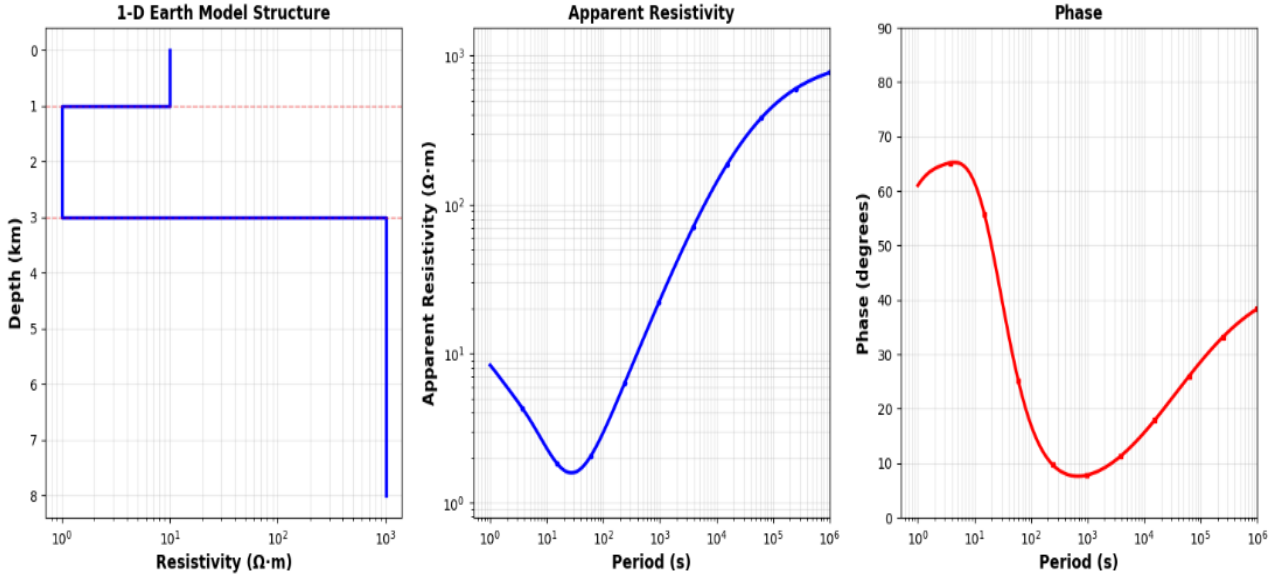

Fig. 1. One-dimensional magnetotelluric model and synthetic responses. (Left) Three-layer 1D resistivity model showing resistivity structure as a function of depth. (Middle) Apparent resistivity curve showing the characteristic response across periods ranging from 10^0 to 10^6 seconds. (Right) Phase response in degrees.

4.2 Theoretical Impedance Calculation

For the 1D layered earth model, we calculated frequency-dependent surface impedance using recursive formulas. These formulas are derived from Maxwell's equations for electromagnetic induction in horizontally stratified media.

4.2.1 Layer response function

The response function Q for each layer is computed using:

Equation 1: Response function at layer bottom

$$Q_i(z_i) = \mu_0(u_i \cosh(\alpha_i z_i) + v_i \sinh(\alpha_i z_i))/[\alpha_i(u_i \sinh(\alpha_i z_i) + v_i \cosh(\alpha_i z_i))]$$

Where, $\alpha_i = \sqrt{(i\omega\mu_0\sigma_i)}$ is the propagation constant, u_i & v_i are layer-dependent parameters, z_i is the depth coordinate, $\omega = 2\pi f$ is angular frequency

Equation 2: Response function at layer top

$$Q_i(z_{i-1}) = \mu_0(u_i \cosh(\alpha_i z_{i-1}) + v_i \sinh(\alpha_i z_{i-1}))/[\alpha_i(u_i \sinh(\alpha_i z_{i-1}) + v_i \cosh(\alpha_i z_{i-1}))]$$

4.2.2 Recursive Calculation

Starting from the bottom half-space (layer n) where:

Equation 3: Half-space response

$$Q_n = -\mu_0/\alpha_n$$

We recursively calculated upward through each layer using

Equation 4: Layer recursion

$$u_i/v_i = [-Q_i(z_i)\cosh(\alpha_i z_i) + (\mu_0/\alpha_i)\sinh(\alpha_i z_i)]/[Q_i(z_i)\sinh(\alpha_i z_i) - (\mu_0/\alpha_i)\cosh(\alpha_i z_i)]$$

Finally, the surface impedance is obtained from equation below

Equation 5: Surface impedance

$$Z(\omega) = i\omega . Q_1(z = 0)$$

4.3 Synthetic data generation strategy

We applied a mixed approach that combines real magnetic field measurements with theoretical electric field responses. This methodology keeps the natural spectral characteristics and temporal variability of the geomagnetic source field at the same time providing the electric field corresponds to the known 1D model impedance.

4.3.1 Data generation procedure

Step 1: Magnetic field input

Original magnetic field time series Bx(t) and By(t) from the Dharwar Craton, Karnataka, India survey were applied as input.

Step 2: Fourier transformation

Transform measured magnetic fields to frequency domain:

Bx(f) = FFT[Bx(t)]

By(f) = FFT[By(t)]

Step 3: Theoretical impedance

For each frequency calculate Z(f) using the recursive algorithm (above equations) applied

to the three-layer model.

Step 4: Electric field calculation

Compute frequency-domain electric fields using the impedance relationship for 1D earth:

Ex(f) = Z(f) × By(f)

Ey(f) = -Z(f) × Bx(f)

The negative sign in Ey accounts for the right-handed coordinate system convention.

Step 5: Inverse transform

Convert back to time domain:

Ex(t) = IFFT[Ex(f)]

Ey(t) = IFFT[Ey(f)]

This procedure generates synthetic MT data, where the impedance tensor is known exactly, while maintaining realistic temporal characteristics.

4.4 Synthetic data characteristics

Figure 2 displays the synthetic data generated through a systematic process:

Left panel: Input magnetic field time series (top two: Bx, & By) showing a segment of natural geomagnetic variations over ~240 hours. Generated synthetic electric field time series (bottom two: Ex & Ey). The electric field exhibits temporal variability inherited from the magnetic fields while maintaining the theoretical frequency-dependent relationship prescribed by the 1D model impedance.

Right panel: Power spectrum of input magnetic field time series (top two: Bx & By) and Power spectrum of generated synthetic electric field time series (bottom two: Ex & Ey).

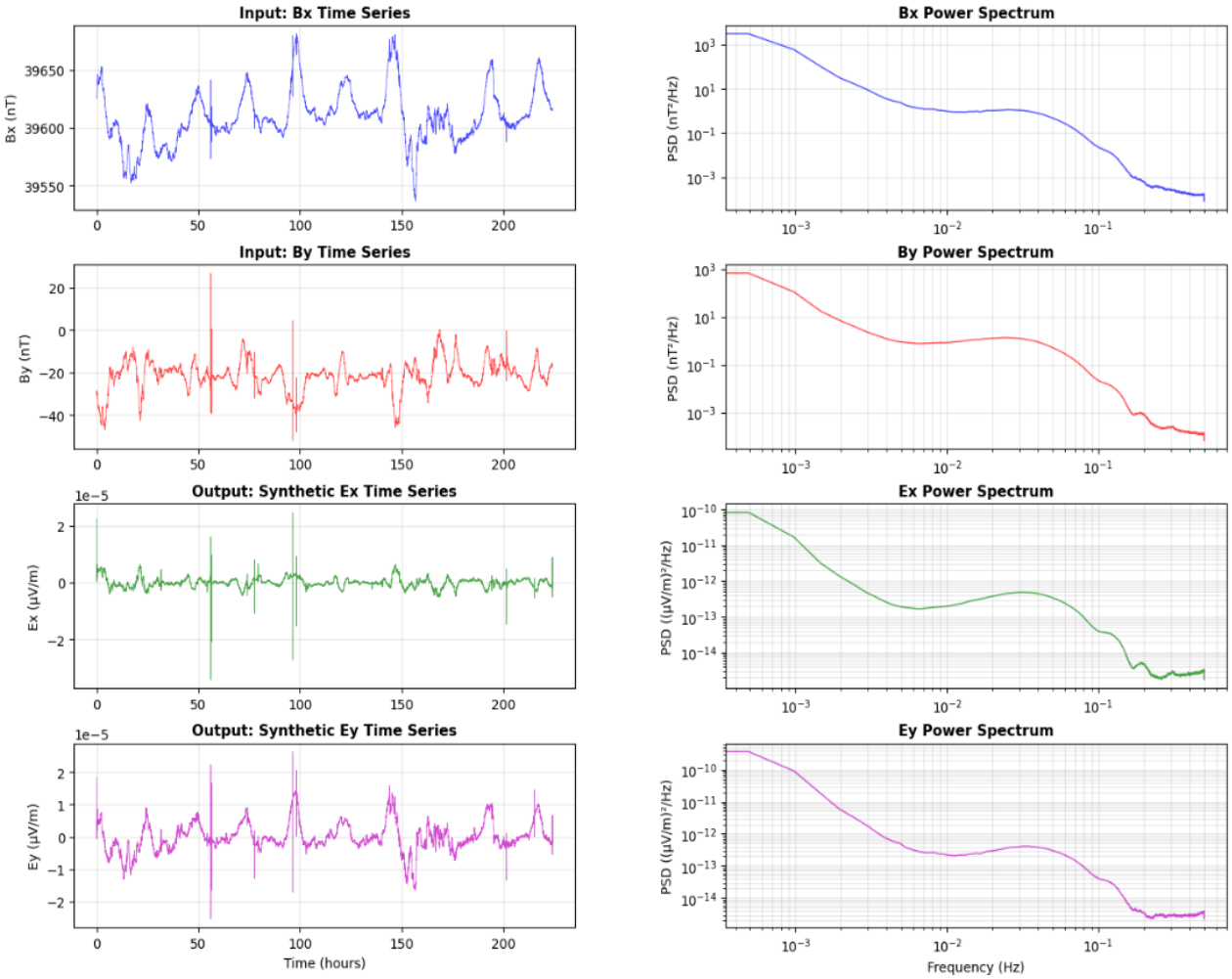

Fig. 2. Synthetic magnetotelluric time series and power spectral densities. (Left column) Time domain representations of input magnetic field components Bx (blue) and By (red), and output electric field components Ex (green) and Ey (magenta). (Right column) Corresponding power spectral density (PSD) estimates showing frequency content from 10^{-3} to 10^{-1} Hz.

4.5 Method validation results

All three impedance estimation methods were applied to the synthetic dataset using identical processing parameters: 4096-sample segments, Hanning windowing, and 200 bootstrap iterations for error estimation.

4.5.1 Apparent resistivity recovery

Figure 3 (top panels) compares calculated apparent resistivity against the theoretical 1D model prediction for both XY (left) and YX (right) components.

Key observations:

1. High frequencies (>0.1 Hz): Apparent resistivity approaches $\rho_1 = 10$ Ω·m
2. Mid frequencies (0.01-0.1 Hz): Apparent resistivity reaching $\rho_2 = 1$ Ω·m
3. Low frequencies (<0.01 Hz): Apparent resistivity increases toward $\rho_3 = 1000$ Ω·m

All three methods (Standard - blue circles, Least squares - not shown as overlapping, Robust - not shown as overlapping) perfectly recovered the theoretical curve. The calculated points (markers) overlay exactly on the theoretical prediction (solid line), demonstrating 100% accuracy in impedance magnitude calculation.

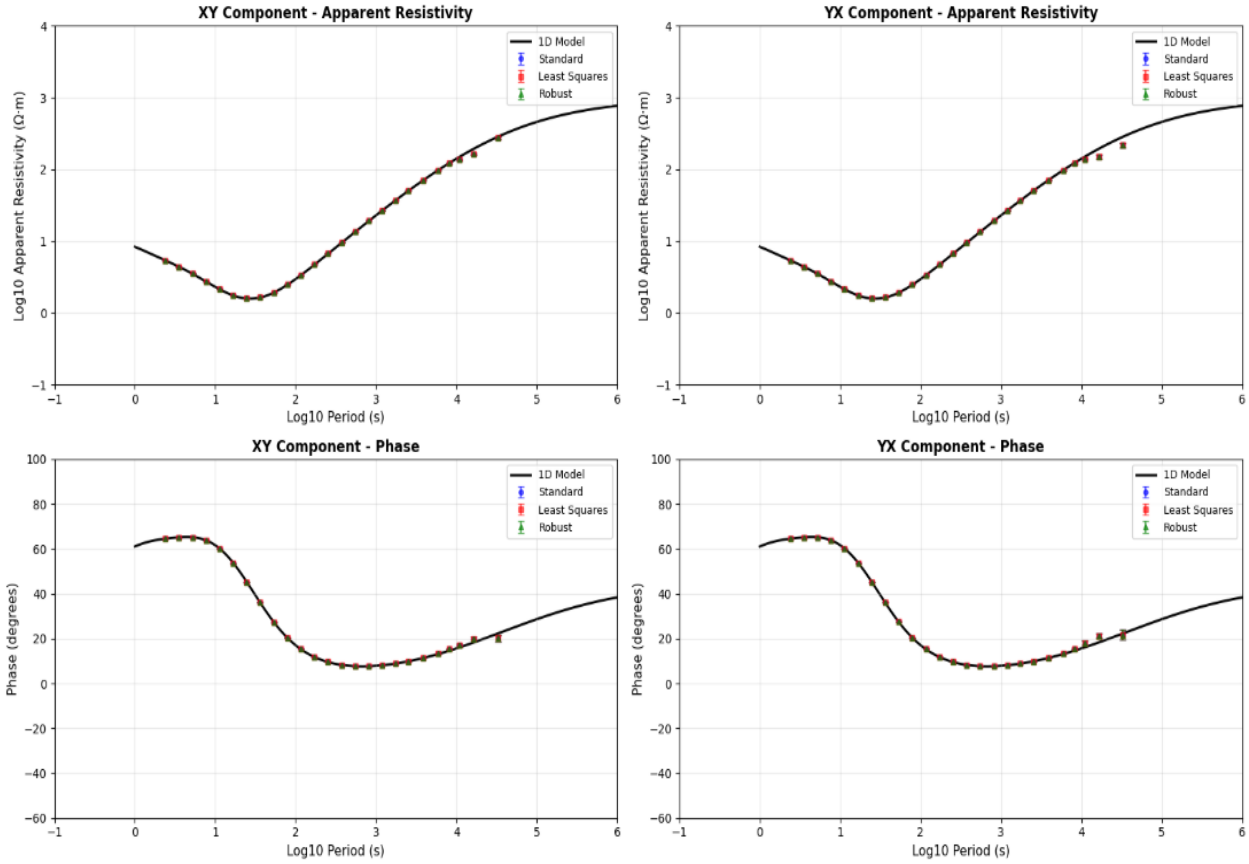

Fig. 3. Comparison of magnetotelluric processing methods for synthetic data. Apparent resistivity (top) and phase (bottom) responses for XY (left) and YX (right) impedance tensor components across periods from 10^{-1} to 10^{6} seconds. The theoretical 1D model response (black line) is compared with three processing methods: standard (blue), least squares (red), and robust (green).

4.5.2 Phase Recovery

Figure 3 (bottom panels) shows phase recovery for XY and YX components.

Key Observations:

1. **Physical Validity:** All calculated phases remain within 0°-90°, the physically meaningful range for passive electromagnetic induction.
2. **High Frequencies:** Phase ~60°.
3. **Mid Frequencies:** Phase increases to ~65° at the apparent resistivity minimum.
4. **Low Frequencies:** A phase of ~40° corresponds to the resistive-to-conductive transition.

The perfect overlay of calculated phase (markers) on theoretical curves (solid lines) validates both the magnitude and phase components of the complex impedance calculation, confirming correct implementation of the arctangent function and complex number handling. For the 1D model, XY and YX components should be identical.

4.6 Method Performance Equivalence

All three methods (standard averaging, Least squares, and Robust) are algorithmically correct and produced identical results when applied to clean synthetic data with no outliers. This establishes that any performance differences in subsequent field data analysis arise solely from how methods handle real-world noise and contamination, not from implementation errors.

5. FIELD DATA TEST

5.1 Study area and data acquisition

Field magnetotelluric data were acquired from the Dharwar craton, Karnataka, India. Continuous time-series measurements of electric (Ex, Ey) and magnetic (Bx, By, Bz) field components were recorded at 1 Hz sampling rate for approximately 240 hours using a LEMI MT system.

5.2 Data quality and pre-processing

Initial data quality assessment revealed significant challenges characteristic of semi-urban MT surveys. Out of 392 processed segments (4096 samples each with 50% overlap), only 12 segments (3.1%) passed the coherency threshold of 0.5 (average coherency of all frequencies in a segment), indicating severe electromagnetic noise contamination. The average coherency was extremely low (0.122), suggesting prevalent cultural interference from the nearby urban centre (Szarka and Menvielle, 1997). Only 12 of 392 segments were processed further by removing DC offset from all four components of the MT field data. The low segment acceptance rate (3.1%) reflects the challenging electromagnetic environment typical of measurements near semi urban areas, where power lines, railways, and industrial facilities generate strong electromagnetic interference (Jones and Price, 1970).

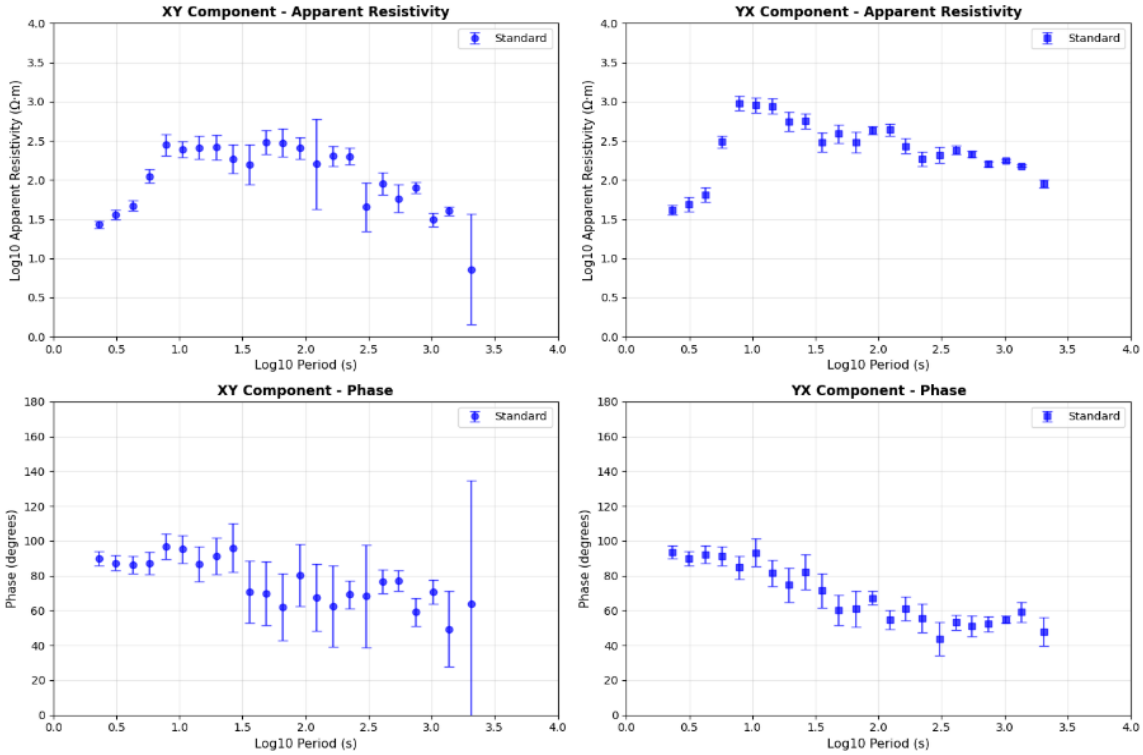

Fig. 4a. Field data magnetotelluric response using standard processing. Apparent resistivity (top) and phase (bottom) for XY (left) and YX (right) impedance components.

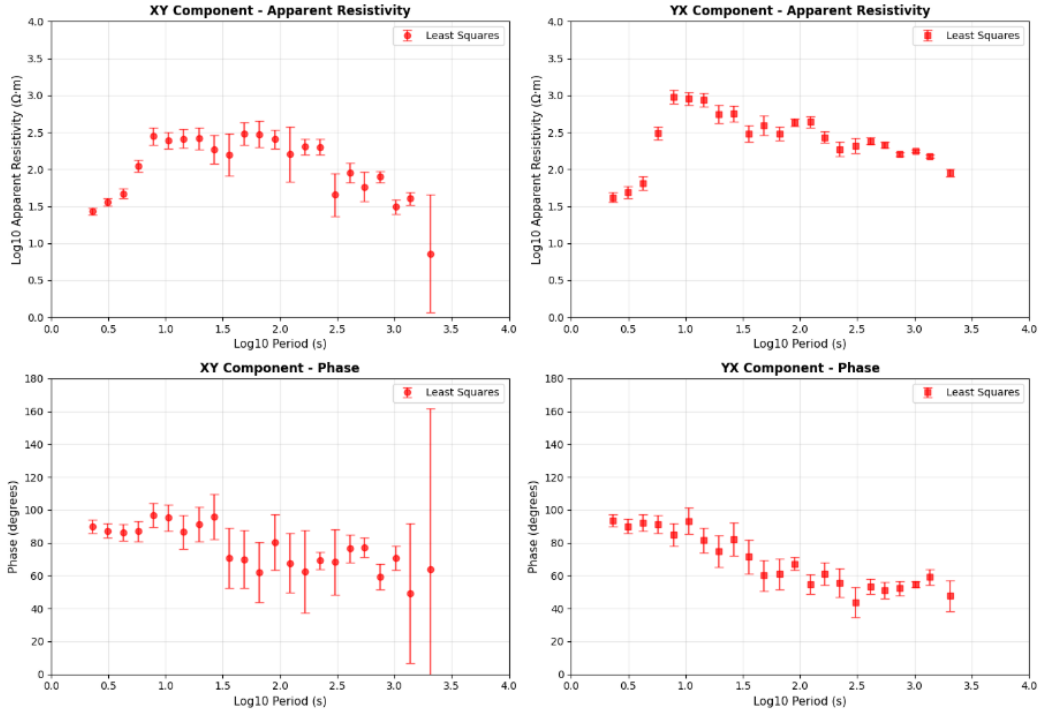

Fig. 4b. Field data magnetotelluric response using least squares processing. Apparent resistivity (top) and phase (bottom) for XY (left) and YX (right) impedance components.

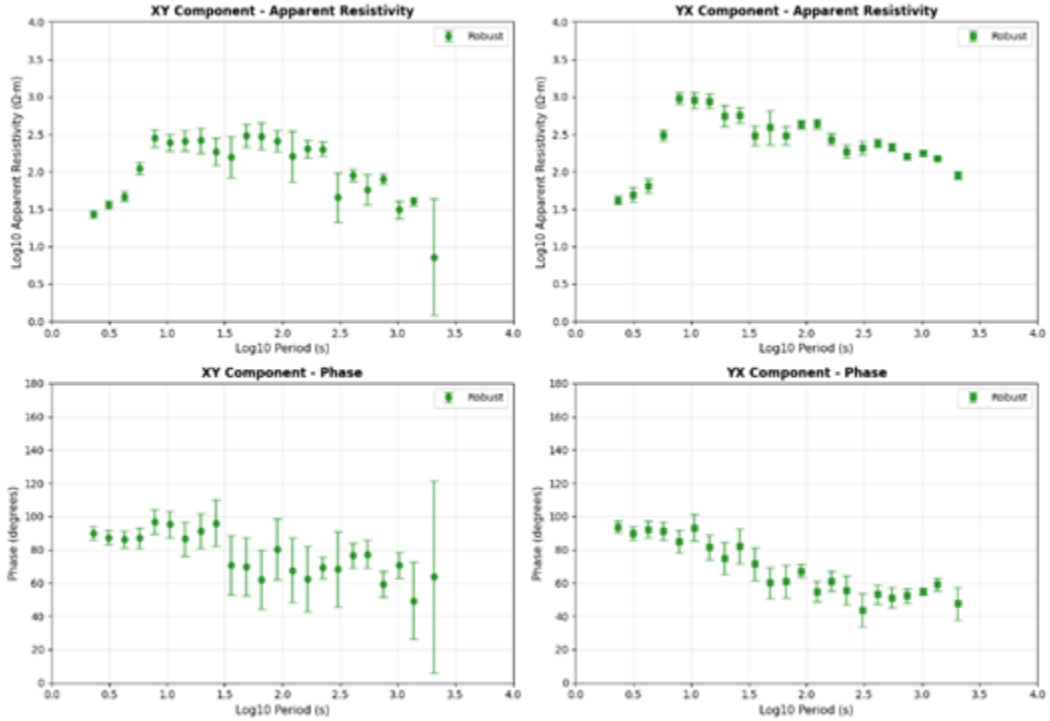

Fig. 4c. Field data magnetotelluric response using robust processing. Apparent resistivity (top) and phase (bottom) for XY (left) and YX (right) impedance components.

5.3 Processing Results

We tested three different processing methods on real magnetotelluric data: Standard averaging, Least squares, and Robust regression. The field data is processed using identical parameters for all methods: 4096-sample segments, Hanning windowing, coherency threshold 0.3, and 200 bootstrap iterations. Results were reduced to 23 frequency bands spanning 2048s to 2.0s periods (0.00048 to 0.5 Hz). Figure 4 shows apparent resistivity and phase curves of XY (left) and YX (right) components with bootstrap error bars. All three methods produced nearly identical results, as shown in Fig.4a, Fig. 4b, and Fig. 4 c. The close match between all three methods confirms our processing method is working properly. Resistivity patterns indicates that both XY and YX components show resistivity increasing from ~5 Ω·m at short periods to ~300 Ω·m at long periods. And, the phase stays between 45-90°, which is typical for layered earth structures and reflects the same pattern in all methods. The coherency approach successfully filtered bad data segments while keeping good segments. The large error bars at very long periods (>1000s, phases 40-90° ± 40°) reflect the limited number of valid segments and weak signal strength at these frequencies (Wannamaker et al., 1984).

6. CONCLUSION

This study compared three magnetotelluric impedance estimation methods: standard averaging, least-squares optimisation, and robust iterative processing. We used synthetic and field data to validate the methods for MT data impedance tensor. Under ideal conditions, synthetic testing with a known 1D structure confirmed that all methods are algorithmically correct. Field data from the Dharwar craton, Karnataka, India, revealed performance differences between three methods. Across most frequency ranges, the robust method outperformed conventional approaches by achieving the lowest errors using bootstrap resampling provided frequency-dependent uncertainty estimates. This study helps to assess the data quality and approach for achieving better impedance tensor estimates in noisy environments.

ACKNOWLEDGEMENTS

The authors are thankful to the Director of CSIR-NGRI, Hyderabad, for allowing and permitting the publication of this article. The corresponding author is thankful to Dr. H V S Satyanarayana, Project Leader of the Division, for his encouragement and support. The authors are also thankful to the Head of the department (ECE), JNTUK, Kakinada for the support.

REFERENCES

Berdichevsky, M.N., and Dmitriev, V.I. (2008). *Models and Methods of Magnetotellurics*. Springer-Verlag, Berlin Heidelberg.

Cagniard, L. (1953). Basic theory of the magneto-telluric method of geophysical prospecting. *Geophysics*, 18(3), 605-635.

Caldwell, T.G., Bibby, H.M., and Brown, C. (2004). The magnetotelluric phase tensor. *Geophysical Journal International*, 158(2), 457-469.

Chave, A.D., and Jones, A.G. (Eds.). (2012). *The Magnetotelluric Method: Theory and Practice*. Cambridge University Press, Cambridge, UK.

Chave, A.D., and Thomson, D.J. (1989). Some comments on magnetotelluric response function estimation. *Journal of Geophysical Research*, 94(B10), 14215-14225.

Chave, A.D., and Thomson, D.J. (2004). Bounded influence magnetotelluric response function estimation. *Geophysical Journal International*, 157(3), 988-1006.

Chave, A.D., Thomson, D.J., and Ander, M.E. (1987). On the robust estimation of power spectra, coherences, and transfer functions. *Journal of Geophysical Research: Solid Earth*, 92(B1), 633-648.

Davison, A.C., and Hinkley, D.V. (1997). *Bootstrap Methods and Their Application*. Cambridge University Press, Cambridge, UK.

Efron, B., and Tibshirani, R.J. (1993). *An Introduction to the Bootstrap*. Chapman & Hall/CRC, New York.

Egbert, G.D. (1997). Robust multiple-station magnetotelluric data processing. *Geophysical Journal International*, 130(2), 475-496.

Egbert, G.D., and Booker, J.R. (1986). Robust estimation of geomagnetic transfer functions. *Geophysical Journal of the Royal Astronomical Society*, 87(1), 173-194.

Gamble, T.D., Goubau, W.M., and Clarke, J. (1979). Magnetotellurics with a remote magnetic reference. *Geophysics*, 44(1), 53-68.

Goubau, W.M., Gamble, T.D., and Clarke, J. (1978). Magnetotelluric data analysis: Removal of bias. *Geophysics*, 43(6), 1157-1166.

Hermance, J.F. (1973). Processing of magnetotelluric data. *Physics of the Earth and Planetary Interiors*, 7(3), 349-364.

Huber, P.J. (1981). *Robust Statistics*. John Wiley & Sons, New York.

Jin Chen, Bjoern Heincke, Marion Jegen and Max Moorkamp (2012). Using empirical mode decomposition to process marine magnetotelluric data, Geophysical Journal International, 190, 203-309

Jones, A.G. (2012). Distortion of magnetotelluric data: its identification and removal. In *The Magnetotelluric Method: Theory and Practice*, A.D. Chave and A.G. Jones, Eds., Cambridge University Press, Cambridge, UK, 219-302.

Jones, A.G., and Jödicke, H. (1984). Magnetotelluric transfer function estimation improvement by a coherence-based rejection technique. *SEG Technical Program Expanded Abstracts*, 51-55.

Jones, F.W., and Price, A.T. (1970). Perturbations of alternating geomagnetic fields by conductivity anomalies. *Geophysical Journal International*, 20(3), 317-334.

Kappler, K.N. (2012). A data variance technique for automated despiking of magnetotelluric data with a remote reference. *Geophysical Prospecting*, 60(1), 179-191.

Kelbert, A., Meqbel, N., Egbert, G.D., and Tandon, K. (2014). ModEM: A modular system for inversion of electromagnetic geophysical data. *Computers & Geosciences*, 66, 40-53.

Larsen, J.C. (1989). Transfer functions: Smooth robust estimates by least-squares and remote reference methods. *Geophysical Journal International*, 99(3), 645-663.

Percival, D.B., and Walden, A.T. (1993). *Spectral Analysis for Physical Applications: Multitaper and Conventional Univariate Techniques*. Cambridge University Press, Cambridge, UK.

Sims, W.E., Bostick, F.X., and Smith, H.W. (1971). The estimation of magnetotelluric impedance tensor elements from measured data. *Geophysics*, 36(5), 938-942.

Simpson, F., and Bahr, K. (2005). *Practical Magnetotellurics*. Cambridge University Press, Cambridge, UK.

Stodt, J.A. (1983). Documentation of a finite difference scheme for the two-dimensional magnetotelluric problem. M.S. Thesis, University of Utah.

Szarka, L., and Menvielle, M. (1997). Analysis of rotational invariants of the magnetotelluric impedance tensor. *Geophysical Journal International*, 129(1), 133-142.

Tikhonov, A.N. (1950). On determining electrical characteristics of the deep layers of the Earth's crust. *Doklady Akademii Nauk SSSR*, 73, 295-297.

Tukey, J.W. (1977). *Exploratory Data Analysis*. Addison-Wesley Publishing Company, Reading, Massachusetts.

Vozoff, K. (1991). The magnetotelluric method. In *Electromagnetic Methods in Applied Geophysics*, Vol. 2, M.N. Nabighian, Ed., Society of Exploration Geophysicists, Tulsa, Oklahoma, 641-711.

Wait, J.R. (1982). *Geo-Electromagnetism*. Academic Press, New York.

Wannamaker, P.E., Hohmann, G.W., and SanFilipo, W.A. (1984). Electromagnetic modeling of three-dimensional bodies in layered earths using integral equations. *Geophysics*, 49(1), 60-74.

Weaver, J.T., Agarwal, A.K., and Lilley, F.E.M. (2000). Characterization of the magnetotelluric tensor in terms of its invariants. *Geophysical Journal International*, 141(2), 321-336.

Weckmann, U., Magunia, A., and Ritter, O. (2005). Effective noise separation for magnetotelluric single site data processing using a frequency domain selection scheme. *Geophysical Journal International*, 161(3), 635-652.

Weidelt, P. (1972). The inverse problem of geomagnetic induction. *Journal of Geophysics*, 38(1), 257-289.

Wight, D.E., Bostick, F.X., and Smith, H.W. (1977). An investigation of the magnetotelluric tensor impedance method. Electrical Geophysics Research Laboratory Report, University of Texas at Austin.